

# MedChemComm

Accepted Manuscript



This is an *Accepted Manuscript*, which has been through the Royal Society of Chemistry peer review process and has been accepted for publication.

*Accepted Manuscripts* are published online shortly after acceptance, before technical editing, formatting and proof reading. Using this free service, authors can make their results available to the community, in citable form, before we publish the edited article. We will replace this *Accepted Manuscript* with the edited and formatted *Advance Article* as soon as it is available.

You can find more information about *Accepted Manuscripts* in the [Information for Authors](#).

Please note that technical editing may introduce minor changes to the text and/or graphics, which may alter content. The journal's standard [Terms & Conditions](#) and the [Ethical guidelines](#) still apply. In no event shall the Royal Society of Chemistry be held responsible for any errors or omissions in this *Accepted Manuscript* or any consequences arising from the use of any information it contains.

## ARTICLE

## Sustained anti BCR-ABL activity with pH responsive Imatinib Mesylate loaded PCL nanoparticles in CML cells

Cite this: DOI: 10.1039/x0xx00000x

Barbara Cortese,<sup>a,b</sup> Stefania D'Amone,<sup>a</sup> Giuseppe Gigli<sup>a,c,d</sup> and Ilaria Elena Palamà<sup>a\*</sup>

Received 00th January 2012,  
Accepted 00th January 2012

DOI: 10.1039/x0xx00000x

[www.rsc.org/](http://www.rsc.org/)

Imatinib Mesylate (IM) is an inhibitor that targets the tyrosine kinase activity of BCR-ABL present in Chronic Myeloid Leukemia (CML). Here, IM-Chitosan complexes loaded poly( $\epsilon$ -caprolactone) (PCL) nanoparticles (NPs) are recommended for its potential in supporting controlled release and improving chemotherapeutic efficiency of IM. The nanoparticles with a size of about 247 nm has a core-shell structure with IM-containing inner core surrounded by PCL layer. The presence of chitosan (CH) allows one to modulate the release kinetics in the pH-dependent manner. IM is released from the NPs much more quickly at pH 4.0 and 6.0 than at pH 7.4, which is a desirable characteristic for cancer-targeted drug delivery. Our core-shell PCL NPs could provide simple and easy way to allow controlled release of IM and improve its chemotherapeutic efficiency, combining the pH sensibility of CH and the slow degradation of PCL.

### Introduction

CML is a hematologic malignancy that is recognized by the presence of Philadelphia (Ph) chromosome which is the result of a reciprocal chromosomal translocation t(9;22) in hemopoietic cells.<sup>1,2</sup> BCR-ABL, a constitutively active protein kinase, is the product of Ph chromosome and plays a key role in the pathogenesis of CML, likely via phosphorylation of multiple downstream protein targets, resulting in the activation of cellular pathways and therapeutic resistance. The introduction of the tyrosine-kinase inhibitor (TKI) Imatinib Mesylate (IM, STI571, Gleevec) in the treatment of CML has been a major medical breakthrough in controlling this disease.<sup>3</sup> Nevertheless, a subpopulation of BCR-ABL+ cells in the niche are found which display stem cell-like features, such as self-renewal and quiescence.<sup>4,5,6,7</sup> These CML stem cells are shown to be unresponsive to TKI treatment and are capable of deriving the disease during the relapse. This leads to IM dose escalation or early disease relapses when therapy is stopped or discontinued. Potential risks of adverse effects with long-term treatment with IM have refocused the interest of researchers towards nanocarriers for delivery to increase drug's retention effects<sup>8</sup> and antileukemic activity in viable residual CML cells. In this context, we have previously validated two types of polymeric vectors for IM delivery to CML cells. IM-loaded polyelectrolyte microcapsules were validated as effective purging agents to eradicate positive BCR-ABL cells from CML patients.<sup>9</sup> Then, we have also validated a IM loaded polyelectrolyte nanocomplexes (PECs) as effective carriers to maximize the apoptotic effects of IM in CML cells, at a tenfold lower dose compared with that reaching 50% cell viability inhibition *in vitro*.<sup>10,11</sup> IM-loaded PECs, in marrow CD34+ cells derived by CML patients, have enhanced antileukemic effects compared with the same concentration of free IM. The better efficacy of IM-PECs

in promoting a constant inhibition of BCR-ABL in a more effective fashion compared with IM-loaded polyelectrolyte microcapsules could reveal their capacity to delay with cytosolic and nuclear BCR-ABL activity.

In recent years, more attention has been directed to stimuli-sensitive drug delivery systems that are a promising strategy for drug release.<sup>12</sup> Many techniques have been developed to produce systems that could be used for effective encapsulation of active agents, as drugs or genes.<sup>13,14,15,16</sup> More studies, for example, were focused on delivery systems that could be simply extravasated from the blood vessels and deliver the loaded drugs to cancer cells by improved permeability and retention effect during cancer chemotherapy.<sup>17</sup> In particular, external and internal stimuli, as temperature,<sup>18</sup> pH,<sup>19,20</sup> light,<sup>21</sup> and protease<sup>22</sup> could be utilized to control the drug release in delivery systems.<sup>23</sup> Among all these strategies, release systems based on pH variation has obtained more attention, in particular in cancer therapy field, because the pH difference between normal and tumour cells could be used for targeting drug design. The pH values in the human body naturally varies between the different organs and tissues, which make the pH-triggered approach one of the most efficient strategies for drug delivery.<sup>24</sup> With this aim, in this work we explore a novel IM delivery system based on a pH responsive core shell nanoparticles. An attractive polymer for drug delivery application is the poly( $\epsilon$ -caprolactone) (PCL), approved by the Food and Drug Administration (FDA). PCL nanoparticles are promising for their high colloidal stability in biological fluid, facile cellular uptake, low toxicity *in vitro* and *in vivo*, slow degradation and controlled release.<sup>25</sup>

The PCL NPs, obtained by the emulsion-diffusion-evaporation method, are composed by a core with the IM and a PCL shell. Prior to particle assembly, IM was complexes with chitosan (CH), a polycation widely used as a matrix in drug release systems based on

pH variation.<sup>26</sup> Our core-shell PCL NPs could provide simple and easy way to enable controlled release of IM and improve its therapeutic efficiency, by combining the pH sensibility of CH and the slow degradation of PCL. In addition PVA coating of PCL NPs is used to increase colloidal stability.

The physicochemical properties of the NPs were characterized by using various techniques. The loading efficiency and release kinetics were analysed under different physiological conditions. Cellular uptake and cytotoxicity of PCL NPs were evaluated on CML and healthy cells.

## Materials and methods

### Materials

All tissue culture media and serum were purchased from Sigma-Aldrich, cell lines were purchased from American Tissue Type Collection (ATCC). The suppliers of the chemicals were as follows and were supplied by Sigma-Aldrich: thiazolyl blue tetrazolium bromide (MTT), ethidium bromide (EtBr), Acridine orange (AO), HOECHST 33342, anti-clathrin light chain monoclonal antibody, Fluoroshield with DAPI, Chitosan (CH) low molecular range with degree of deacetylation 75–85%, Poly(-caprolactone) (PCL) with an average molecular weight (MW) of 14.800 Da, Polyvinyl alcohol (PVA, MW 13–23 kDa, 87–80% hydrolyzed). MitoTracker, ERTracker, LysoTracker from Life Technology.

### PCL NPs preparation

PCL nanoparticles were prepared by an emulsion-diffusion-evaporation method. Briefly, a solution of IM (10–100  $\mu$ M) was complexed with a 1% (w/v) chitosan in acetic acid aqueous solution by incubating at room temperature (RT) for 24 hours under stirring. A 100 mg of PCL was dissolved in 10 mL organic phase (9 mL ethyl acetate and 1 mL acetone) for 1 hour at 30°C. As for the aqueous phase, 100 mg PVA were stirred in 5 mL water at RT until a clear solution was obtained, after, IM-CH complex solution was mixed. The organic phase was passed through a 0.22  $\mu$ m syringe filter and then added drop wise to the aqueous phase under constant stirring. The resulting emulsion was kept under constant agitation at 1000 rpm for 1 hour and was subsequently sonicated for 30 minutes. This colloidal preparation was diluted to a volume of 50 mL by adding water drop wise under stirring conditions (1000 rpm), which resulted in nanoprecipitation. In order to remove the organic solvent and to harden the PCL nanoparticles, the suspension was dried with a rotary evaporator at 50 mbar at 40°C for 20 minutes. Next, the nanoparticle suspension was washed three times with water by centrifugation at 12000 rpm for 10 minutes and then resuspended in water. The finished nanoparticle suspension was stored at 4°C for further use. To determine the concentration of nanoparticles (w/v), this suspension was centrifuged to 12000 rpm for 10 minutes; the supernatant was removed and the pellet was allowed to dry under a nitrogen stream before weighing. For preparing fluorescent CH-FITC or CH-TRITC PCL nanoparticles, a 1 mg/mL CH-FITC or CH-TRITC was added to PCL solution and the formulation was carried out as described earlier. The labeled nanoparticles were stored in the dark at 4°C until use.

### Nanoparticles size, surface charge studies and stability

The particle size and zeta potential were determined by Dynamic Light Scattering (DLS) analysis using a Zetasizer Nano ZS90 (Malvern Instruments Ltd., USA) equipped with a 4.0 mW He-Ne laser operating at 633 nm and an avalanche photodiode detector. Measurements were made at 25°C in aqueous solutions (pH 7). The PCL NPs solution (1 mg/mL) was passed through a 0.45  $\mu$ m pore size filter before measurements and appropriately diluted if necessary according to the instrument's requirements. The stability of IM-CH PCL NPs was tested under physiological conditions. Nanoparticles were incubated in complete RPMI medium at 37°C, and the size variation was measured over a period of 8 days by DLS analysis. Representative measurements of three distinct sets of data have been reported (*Student t-test*,  $P < 0.05$ ).

### Scanning Electron Microscopy (SEM) and Atomic Force Microscopy (AFM)

For SEM and AFM analysis, samples were prepared by applying a drop of the particle suspension to a SiO<sub>2</sub> wafer and then drying overnight. Prior to SEM (RHAIT 150) observation, the samples were sputter-coated with a 10 nm gold layer to make them electronically conductive and to avoid electronic charging during SEM imaging. The morphological characterization has been performed by tapping mode AFM using a Solver PRO Scanning Probe Microscope (NT-MDT) in air at room temperature, we used TESPA (Veeco, USA) silicon cantilevers of 20–80 N/m spring constant and resonance frequency of around 300 kHz.

### Determination of drug loading and *in vitro* drug release

The nanoparticles drug loading efficacy was determined by evaluating IM content present in the supernatant of nanoparticle suspension (100  $\mu$ L of supernatant diluted in 1 mL with PBS 1x) were evaluated using an UV–visible spectrophotometer (Varian Cary® 300 Scan; Varian Instruments, CA, USA) at a wavelength of 260 nm. The dose of IM loaded into PCL NPs was calculated using Equation 1:

$$C_c = \frac{(V_i C_i - V_s C_s)}{V_c} \quad (1)$$

Where  $C_c$ ,  $C_i$  and  $C_s$  represent drug concentration in NPs, drug feeding concentration and drug concentration in supernatant after incubation, respectively.  $V_i$ ,  $V_s$  and  $V_c$  refer to the volume of drug feeding solutions, the volume of supernatant and the volume of NPs, respectively. The concentration in supernatant is derived from UV–visible adsorption referring to a standard curve.

Release behaviour of IM from NPs was investigated at pH 4.0 (pH in endosome/lysosomes), pH 6.0 (tumour environment pH), and pH 7.4 (pH of physiological blood). 50 mg of lyophilized IM-CH PCL nanoparticles were dispersed in 5 mL of PBS 1x pH 7.4 and 500  $\mu$ L of sample was dialyzed in a large volume of PBS 1x pH 4.0, pH 6.0 and pH 7.4, and kept at 37°C  $\pm$  0.5°C under stirring at 50 rpm. At specified time intervals, the samples were centrifuged (12000 rpm for 10 minutes) and supernatants were collected. Samples were taken and analysed in triplicates. The concentration of IM release was determined from the corresponding absorbance measured in spectrophotometer at 260 nm. Representative measurements of

three distinct sets of data have been reported (*Student t-test*,  $P < 0.05$ ).

### Cell culture

Human BCR-ABL positive cells (KU812) were established from a CML patient<sup>27</sup> and human normal B lymphoblast (C13589) were cultured in RPMI 1640 (Sigma-Aldrich) containing 10% FBS (Sigma-Aldrich), 100 units/mL penicillin, 100 µg/ml streptomycin and 2 mM l-glutamine (Sigma-Aldrich) at 37°C, 5% CO<sub>2</sub>.

### Cell uptake efficiency of IM loaded NPs

KU812 and C13895 cells were seeded in 24-well plates (10<sup>5</sup> cells/well) in complete culture media and were incubated with drug or drug loaded nanoparticles for 1, 2, 3 and 4 hours, respectively at 37°C. For each sample, we have seeded six wells for positive control and six wells for sample wells. At the selected interval, the sample wells were washed three times with cold PBS 1x. After that, all the wells were lysed by 0.5% Triton X-100 in 0.2 N NaOH solution. The quantity of IM in the cells was fluorometrically determined for the lysate with an excitation wavelength of 254 nm and an emission wavelength of 380 nm using a fluorescence spectrometer. The cellular uptake efficiency was expressed as the percentage of the fluorescence associated with the cells *vs* that present in the positive control cells. Representative measurements of three distinct sets of data have been reported (*Student t-test*,  $P < 0.05$ ).

### Analysis of uptake modality and intracellular localization

KU812 CML cells and C13895 (10<sup>5</sup> cells/mL) were incubated with the FITC PCL NPs dispersions at a concentration of 0.05 mg/mL to determine the cellular uptake of the PCL NPs. After 3 hours of incubation at 37°C, the culture medium was removed, and the cells were washed three times with PBS 1x. For fluorescent microscopic observation, cells were fixed *in situ* for 5 minutes in 3.7% formaldehyde and mounting with fluoroshield with DAPI.

The uptake modality of the PCL NPs was evaluated incubating KU812 cells (10<sup>5</sup> cells/mL) with 0.05 mg/mL PCL-TRICT NPs for 1-3 hours, then washed three times with 0.27% glucose/PBS and fixed in ice-cold methanol. After several washes with PBS, cells were incubated at RT for 50 min. with blocking buffer (PBS with 4% horse serum, 0.3% Triton X-100 and 1% BSA) to block non-specific binding. They were then incubated with anti-clathrin light chain monoclonal antibody (10 µg/mL; Sigma-Aldrich) at 37°C for 1 hour. The primary antibody was revealed using Fluorescein isothiocyanate conjugated anti-mouse antibody (4 µg/ml; Millipore, MA, USA) as secondary antibody and mounting with fluoroshield with DAPI.

To study the intracellular localization of FITC-PCL NPs immunostaining with LysoTracker Red (Life technology), MitoTracker Red (Life technology) and ER-Tracker Red (Life technology) were performed, in according with manufacturer's instructions, to label lysosomes, mitochondria and endoplasmic reticulum, respectively. Confocal micrographs were taken with Leica confocal scanning system mounted into a Leica TCS SP5 (Leica Microsystem GmbH, Mannheim, Germany), equipped with a 63 X oil immersion objective and spatial resolution of approximately 200 nm in x-y and 100 nm in z.

### Quantitative analysis of colocalization

For colocalization analysis ten different fields were randomly selected for each sample, and three distinct experiments were performed. We employed the coefficient of correlation (CC or Pearson's  $r$ ),<sup>28</sup> intensity correlation quotient (ICQ)<sup>29</sup> and overlap coefficient (OC)<sup>30</sup> as indices of the frequency of colocalization between PCL NPs and LysoTracker, MitoTracker and ER-Tracker. These indices are all based on pixel-based quantitative analysis of confocal images. CC immunofluorescence signals in the confocal images can range from -1 to 1, where 1 means perfect overlap, and 0 means random distribution. ICQ for the fluorescence signals can show a range from -0.5 to 0.5, where 0.5 means perfect overlap, and 0 means random overlap. OC for the fluorescence signals can range from 0 to 1, where 0 means no overlap, and 1 indicates perfect overlap.

In 12-bit confocal images, pixels with an intensity of 0 or 4095 are deemed to be lacking linearity of fluorescence signals. We therefore carefully determined gain and offset values not to contain pixels with 0 or 4095 intensity when capturing confocal images. Only a few pixels with 0 or 4095 intensity in the red or green colour channels were excluded from calculation of CC, ICQ and OC. It has been reported that exclusion of such pixels improves fidelity of quantitative co-localization analysis.<sup>31</sup> For objective selection of the pixels, we defined thresholds according to background immunofluorescence measured from the negative control sections. Because the maximum intensity in an image of control sample fluctuated between images presumably due to thermal noise arising in the photon detector, we instead used the 999/1000 quantile of intensity (i.e. the highest intensity after removal of the highest 0.1% of data) in each colour channel as the thresholds, we defined the threshold of each colour channel to be the mean value from three images of the control sections. Randomized confocal images were prepared by shuffling of pixels within an image and used for calculation of the coefficients and quotients, as described elsewhere.<sup>32</sup> After the exclusion of pixels unsuitable for the present analysis, shuffling was done only for pixels in the green channel of an image, and the shuffled pixels were paired with pixels in the unchanged red channel. For each confocal image, shuffling was repeated three times, and the mean of coefficients from the three shuffled data was calculated as a representative value for the image unless otherwise stated. All the calculations of coefficients and quotients from each confocal image, as well as pixel shuffling and calculation of the 999/1000 quantile of intensity, were done with custom-made plug-in programs (available at <http://www.mbs.med.kyoto-u.ac.jp/imagej/index.html>) combined with ImageJ software (National Institute for Health, Bethesda, MD, USA). The numerical data were imported to Excel software (Microsoft, Redmond, WA, USA) for further calculation and the results were plotted into graphs. Representative measurements of three distinct sets of data have been reported (*Student t-test*,  $P < 0.05$ ).

### Apoptosis evaluation

KU812 leukemia cells (10<sup>5</sup> cells/mL) were incubated with free IM (10 nM) and IM loaded PCL NPs (10 nM) and after 3 days of incubation, cells were washed and resuspended with PBS 1x. Then, cells were stained with May-Grünwald and Giemsa (Sigma-Aldrich, USA) and were analysed for the morphometric analysis using a light microscope BX61 (Olympus).

The apoptotic cells were evaluated mixing 9 mL of cell suspension ( $10^5$  cells/mL) with 5  $\mu$ L of dye mixture composed by 100 mg/mL Acridine orange (AO) and 100 mg/mL ethidium bromide (EtBr). After 5 minutes of incubation, cells were visualized under fluorescence microscope BX61 (Olympus) with excitation filter at 510-590 nm. The percentage of total apoptotic cells was determined by the Equation 2:

$$\% \text{ of apoptotic cells} = \frac{\text{Total number of apoptotic cells}}{\text{Total number of normal and apoptotic cells}} * 100 \quad (2)$$

Ten different fields were randomly selected for counting 300 cells. Representative measurements of three distinct sets of data have been reported (*Student t-test*,  $P < 0.05$ ).

In addition, apoptosis was investigated by staining the cells with HOECHST 33342 (Sigma-Aldrich, USA). The cells were washed with PBS 1x and then fixed in PBS containing 10% formaldehyde for 2 hours at RT. The fixed cells were washed with PBS 1x, and stained with HOECHST 33342 for 1 hour at RT. The Hoechst-stained nuclei were visualized using a fluorescence microscope BX61 (Olympus) with excitation filter at 358-461 nm.

#### **In vitro cytotoxicity assay**

To test the effect of empty (CH-PCL) or IM loaded NPs on cell growth, 3-[4,5-dimethylthiazol-2-yl]-2,5-diphenyl tetrazolium bromide (MTT) survival tests were performed in accordance to manufacturer's instructions (Sigma-Aldrich, USA). The  $IC_{50}$  of IM was calculated. Briefly, KU812 and C13895 cells were seeded on 24-well plates at a density of  $10^5$  cells/well in complete culture media and NPs were added each well. Untreated samples were used as the control groups. The medium was changed every two days for long time windows of incubations. After an appropriate incubation period, the cultures were removed from the incubator and the MTT solution added in an amount equal to 10% of the culture volume. Then the cultures were returned to the incubator and incubated for 3 hours. After the incubation period, the cultures were removed from the incubator and the resulting MTT formazan crystals were dissolved with acidified isopropanol solution to an equal culture volume. The plates were read within 1 hour after adding acidified isopropanol solution. The absorbance was spectrophotometrically measured at wavelength 570 nm and the background absorbance measured at 690 nm subtracted. The percentage viability is expressed as the relative growth rate (RGR) by Equation 3:

$$RGR (\%) = \frac{D_{\text{sample}}}{D_{\text{control}}} * 100 \quad (3)$$

where  $D_{\text{sample}}$  and  $D_{\text{control}}$  are the absorbances of the sample and the negative control. Representative measurements of three distinct sets of data have been reported (*Student t-test*,  $P < 0.05$ ).

#### **Detection of DNA fragmentation**

KU812 leukemia cells ( $10^6$  cells/mL) were incubated for 12 hours with IM free and IM-CH loaded PCL NPs suspension (10 nM). The control (NT) was complete culture medium only. Then, the cells lysed with lysis buffer (50 mM Tris HCl, pH 8.0, 10 mM ethylenediaminetetraacetic acid, 0.1 M NaCl, and

0.5% sodium dodecyl sulfate). The lysate was incubated with 0.5 mg/mL RNase A at 37°C for 1 hour, and then with 0.2 mg/mL proteinase K at 50°C overnight. Phenol extraction of this mixture was carried out, and DNA in the aqueous phase was precipitated by 1/10 volume of 7.5 M ammonium acetate and 1/1 volume isopropanol. DNA electrophoresis was performed in a 1% agarose gel containing 1  $\mu$ g/mL EtBr at 70 V, and the DNA fragments were visualized by exposing the gel to ultraviolet light, followed by photography.

#### **Validation of BCR-ABL inhibition by Western Blotting**

CML cells incubated for 8 days with IM free or IM-CH loaded PCL NPs were washed in PBS at 4°C and resuspended in lysis buffer (50mM tris HCL, pH 7.4; 1% Triton X-100; 5 mM EDTA; 150 mM NaCl; 1 mM  $Na_3VO_4$ ; 1 mM NaF; 1 mM phenylmethylsulfonyl fluoride), and protease inhibitor cocktail (10  $\mu$ M benzamidine-HCl and 10  $\mu$ g of aprotinin, leupeptin and pepstatin A per mL) followed by incubation on ice for 30 minutes. Lysates were clarified by centrifugation at 13000 rpm for 15 minutes at 4°C and protein concentration was determined using the BCA protein assay (Pierce, IL, USA). Protein bands were separated on SDS-polyacrylamide gels, immunoblotting was performed using Immobilon-P nitrocellulose membrane (Millipore Corp., MA, USA). Primary incubations with anti phosphotyrosine antibody (clone 4G10, Upstate Biotechnology) and anti-c-ABL (clone K-12, Santa Cruz Biotechnology Inc., CA, USA) were performed for 1-3 hours. Secondary incubations were performed for 1 hour with HRP-conjugated anti-mouse or anti-rabbit antibodies (Amersham, IL, USA). Proteins were visualized by chemiluminescence (Super Signal, IL, USA).

## **Results and discussion**

#### **Synthesis and characterization of PCL nanoparticles loaded with IM**

The IM-CH loaded PCL nanoparticles were prepared by emulsion-diffusion-solvent evaporation method. IM-CH complexes were formed in aqueous solution and then were mixed with PVA aqueous solution and this aqueous core was coated with the oil phase containing the PCL molecules.

The nanoparticles observed by AFM and SEM (**Fig. 1A** and **1B**, respectively) have a spherical morphology with a good size distribution. The resulting NPs were characterized for their physicochemical properties, as size and surface zeta potential. As shown in **Fig. 1C**, unloaded PCL nanoparticles had a zeta potential of  $-11.3 \text{ mV} \pm 0.542 \text{ mV}$  and a diameter of  $247.43 \text{ nm} \pm 0.577 \text{ nm}$  (**Fig. 1D**) with a polydispersion index (Pdl) of  $0.334 \pm 0.040$ . Similar size and zeta potential of IM-CH PCL nanoparticles was observed, as shown in **supplementary Fig. S1**.

IM-CH loaded PCL NPs stability was tested under physiological conditions. NPs were incubated in complete RPMI medium at 37°C, and the size variation was measured over a period of 8 days by DLS analysis. As shown in **Fig. 1E**, over a period of 8 days PCL NPs preserve their hydrodynamic size of about 247 nm and no significant change in Pdl was observed, supporting particle stability evidence in physiological settings.

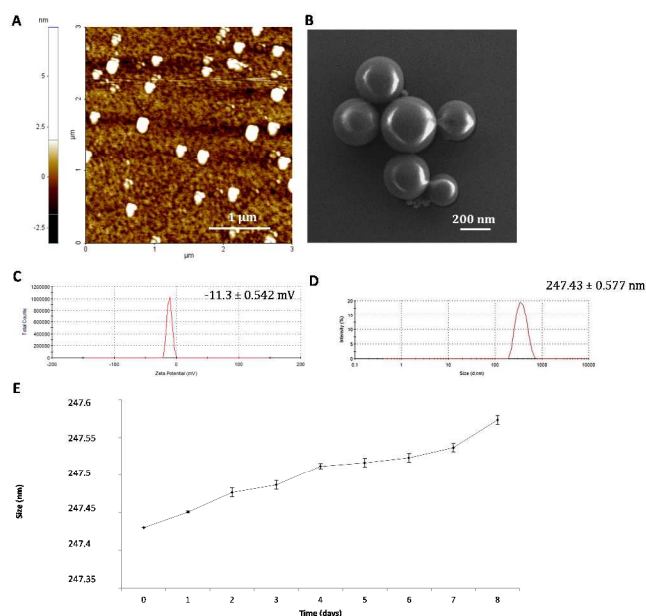


**Fig. 1.** (A) AFM image of dried unloaded PCL NPs. Scale bars: 1  $\mu\text{m}$  (B) SEM image showing the size and morphology of dried unloaded sample. Magnification: 34.01 KX. Scale bars: 200 nm (C) Surface zeta potential distribution demonstrating the uniformity of the sample population. (D) Size distribution from DLS analysis showing the mean  $\pm$  standard deviation of unloaded PCL NPs. Values represents the mean  $\pm$  standard deviation of four independent experiments. (E) Size distribution from DLS analysis showing the incubation effect of IM-CH PCL NPs in complete RPMI medium at 37°C on the NPs stability at different time points. Representative measurements of three distinct sets of data have been reported and no significant difference between values at different time points is observed at  $P < 0.05$  with *t*-Student test.

### IM loading in PCL NPs and drug release kinetics under different physiological conditions

Formulation optimization and purification process led to a high encapsulation efficiency ( $88 \pm 2.5\%$ ) without altering size and sphere-shaped morphology of nanoparticles. Drug content is a crucial problem for a drug delivery system, different IM doses were tested to maximize NPs IM content. After the lyophilisation and re-dispersion, the hydrodynamic size of the IM PCL NPs was scarcely altered and suggesting that the IM-CH loaded PCL NPs has good re-dispersion stability. In addition, it was found that IM loading had insignificant effect either on size and zeta potential possibly because IM is principally dispersed in polymer nanoparticles core (see supplementary **Fig. S1-S2**). Therefore, any additional growth of IM precipitates is prohibited and all IM molecules is immobilized inside the NPs, that leading to high drug encapsulation efficiency.

As shown in **Fig. 2**, IM release was governed by medium pH and release time. Drug release at pH 7.4 was slow and constant, with release percentage at about  $21.65 \pm 0.67\%$  in 192 hours. Conversely, at lower pH, IM release rate was much quicker, with about  $42.79 \pm 0.98\%$  (pH 6.0) and  $62.79 \pm 0.98\%$  (pH 4.0) of the IM released. These different release kinetics are indeed associated to different release mechanisms. At pH 7.4, IM release is governed by the molecules diffusion out of the hydrophilic core, through the holes of the PCL/PVA shell, endorsing that in neutral pH the IM release is determined by passive diffusion through the polymeric shell holes. In contrast, IM/CH complexes protonation at lower pH, is probable linked with the

CH-PCL shell hydrolysis in acid conditions that would gradually increase the nanoparticles permeability with rapid IM release. It can be assumed that most IM will remain in the NPs for a significant time period at normal physiological conditions, demonstrating the potential for prolonged drug retention time in blood circulation and thereby greatly reducing the side effects to normal tissues. Conversely, when IM-loaded chitosan/PCL nanoparticles are engaged by CML cells, a closer release may occur at lower local pH, leading to substantial enhancement in cancer treatment efficacy.<sup>33</sup>

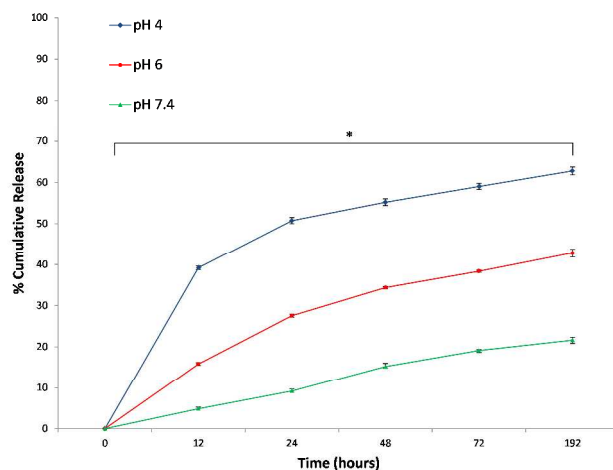


**Fig. 2.** *In vitro* IM cumulative release from CH PCL NPs at neutral condition (pH 7.4) and acidic conditions (pH 6.0 and 4.0) at 37 °C. Representative measurements of three distinct sets of data have been reported and \*indicate  $P$ -values  $< 0.05$  for *t*-Student test between different time points.

### Cellular uptake and intracellular localization

Uptake of CH-PCL NPs in KU812 leukemia cells and in healthy C13895 cells was studied by confocal laser scanning microscopy (CLSM). After 3 hours of incubation, CH-PCL NPs appeared as fluorescent nanodots with a uniform distribution in the cytoplasm and the nucleus (**Fig. 3**). Analogous cellular distribution, we have observed in our previous study on the uptake of polyelectrolytes nanocomplexes (PECs) on CML cells<sup>11</sup> and we previously described that the particles size could influence their uptake modality and the accessibility of IM to cytosolic and/or nuclear pools of BCR-ABL.<sup>9,11</sup>

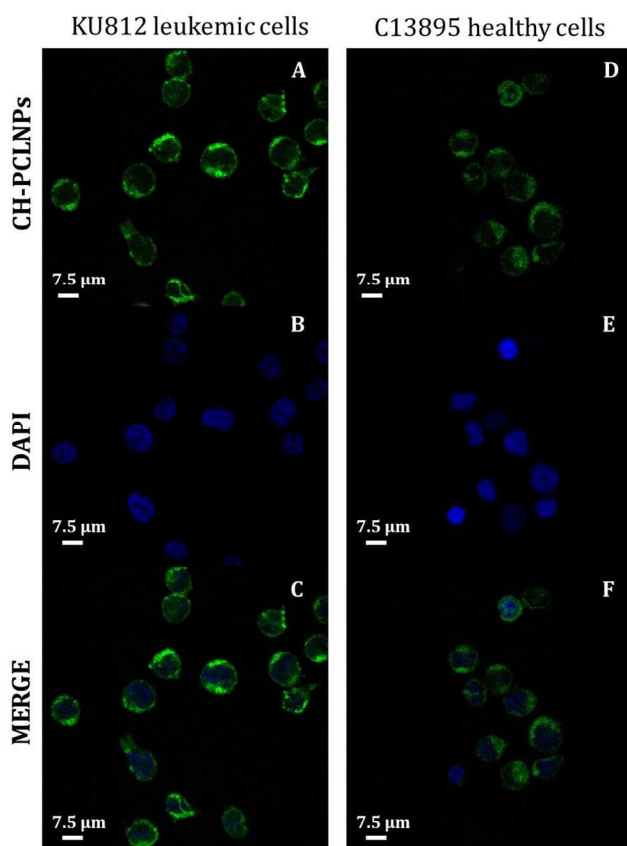


**Fig. 3.** CLSM images of CH-FITC PCL NPs (A,D, green) treated KU812 leukemic cells (A,B,C) and healthy C13895 cells (D,E,F) after 3 hours of incubation. Cell nuclei were counterstained with DAPI (B,E, blue). C,F represent the merged confocal images, with a 63X oil immersion objective. Scale bars: 7.5 μm.

The cellular uptake efficacy of IM-CH loaded PCL NPs was compared with IM alone, used as single agent, after 1,2,3 and 4 hours in culture. It can be seen in **Fig. 4** that the IM-CH loaded PCL NPs revealed enhanced cellular uptake for KU812 and C13895 cells compared with IM free in the medium. It can be seen that IM-CH loaded PCL NPs demonstrated much higher cellular efficiency that the drug only.

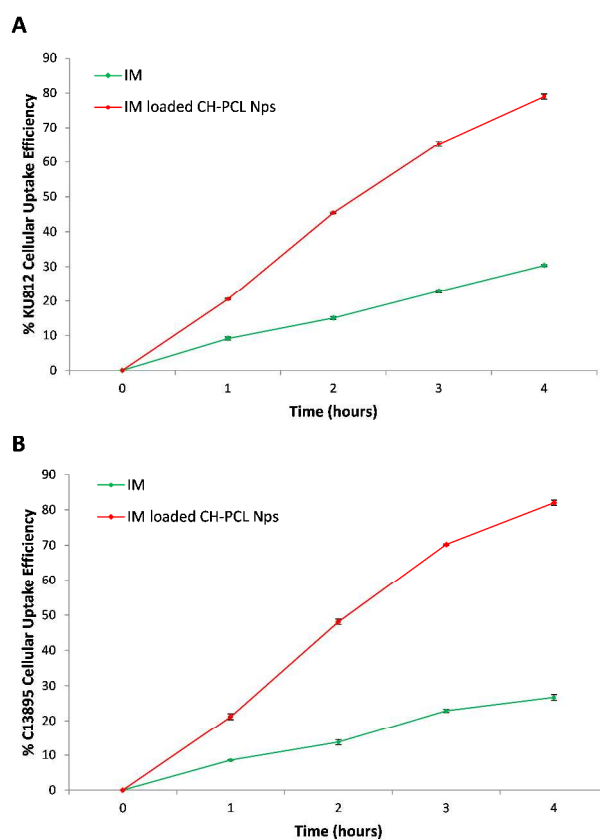


**Fig. 4.** Time-dependent cellular uptake efficiency of IM free and IM-CH loaded PCL NPs by KU812 cells (A) and C13895 cells (B) after 1, 2, 3 and 4 hours of incubation, respectively. Representative measurements of three independent experiments have been reported, no significant difference between values at different time points (*t*-Student test,  $P < 0.05$ ).

For any delivery system, understanding the initial way of internalization is the first step in achieving optimized drug delivery. In this regard, we previously described that the initial uptake of IM-loaded polyelectrolyte microcapsules (3 μm of diameter) was principally nuclear in CML cells.<sup>9</sup> In contrast, nanoscaled PECs (250 nm) were internalized with a clathrin-mediated endocytosis mechanism.<sup>11</sup> This disagreement could be reflected the typical morphological features of CML stem/myeloid cells, which have a condensed cytoplasm and a large nucleus (**Fig. 3**).<sup>34,35</sup> It seems plausible that the uptake of big particles could be facilitated by fusion between the outer plasma membrane and the perinuclear envelope of CML cells through macropinocytosis/phagocytosis,<sup>36</sup> while nanoparticles can be favorably internalized via caveolin/clathrin-mediated endocytosis mechanisms.<sup>37,38,39,40</sup> NPs larger than 20-40 nm are internalized by endocytosis caveolin-mediated, while NPs with variable shape and size are internalized by clathrin-mediated endocytosis mechanisms.<sup>41,42</sup> Our CH-PCL NPs has an average diameters of 247 nm and we guessed clathrin-mediated endocytosis as a accepted internalization mechanism. Our hypothesis was confirmed by observing after 1 hours of CH-PCL NPs incubation inside the cytoplasm a polarized colocalization (**Fig. 5D and supplementary Fig. S6D**) of green clathrin light chain (**Fig. 5A and supplementary Fig. S6A**) and red CH-PCL NPs (**Fig. 5B and supplementary Fig. S6B**) and after 3 hours a redistribution of clathrin inside the cells was evident (**Fig. 5E-H and supplementary Fig. S 6E-H**). These

results suggested the quick induction of clathrin vesicles at the outer plasma membrane in reply to CH-PCL NPs incubation, and their rapid redistribution in specific subcellular compartments.

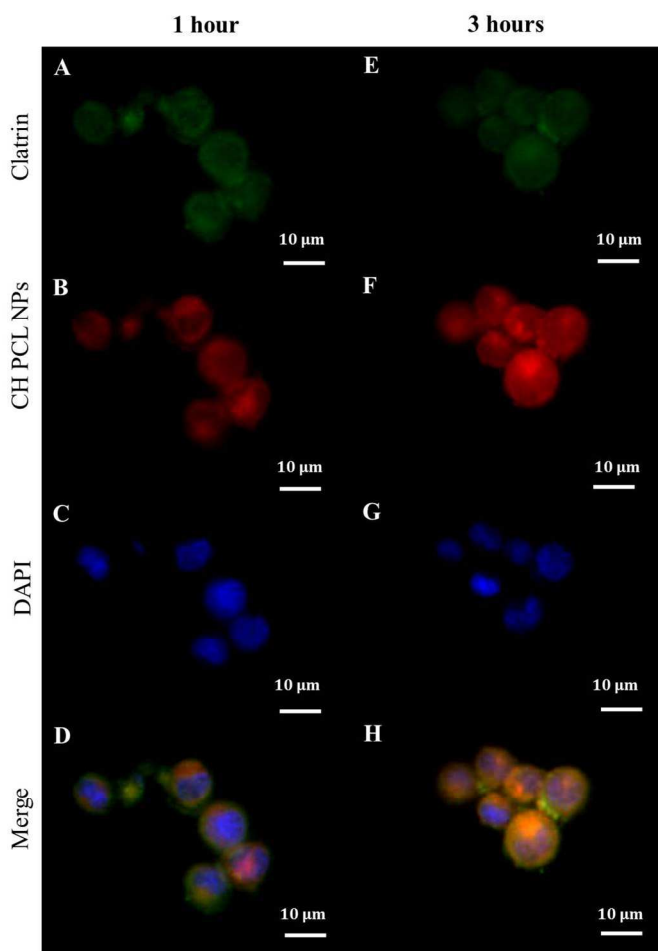


**Fig. 5.** Clatrin (A,E) immunofluorescence (green) in KU812 leukemia cells after 1 (A) and 3 (E) hours of incubation with (B,F) CH-TRITC PCL NPs (red). Cell nuclei (C,G) were counterstained with DAPI (blue). Merge images (D,H) shows colocalization of NPs with clatrin. 63X oil immersion objective. Scale bars: 10  $\mu\text{m}$ .

As shown in **Fig.6 and in supplementary Fig. S7**, NPs were principally transported to mitochondria and lysosome, as evident by high colocalization (yellow present in the merge channel of CLSM images of **Fig. 6D, 6L and in supplementary Figure S7D,L**) of green fluorescence CH-FITC PCL NPs and red fluorescence of MitoTracker and LysoTracker marker. In opposition, low colocalization with red fluorescence of ERTracker was observed, and this indicates that the NPs is not typically localized within endoplasmic reticulum. In particular, in **supplementary Figure S8** a quantitative colocalization analysis between PCL NPs and LysoTracker, MitoTracker and ER-Tracker for KU812 leukemia cells (**supplementary Figure S8A**) and C13895 healthy cells (**supplementary Figure S8B**) is shown. The coefficient of correlation (CC, typically in the range -1 and 1, where 1 means perfect overlap, and 0 means random distribution) between PCL NPs and LysoTracker or MitoTracker was around  $0.61 \pm 0.02$  and  $0.67 \pm 0.02$  respectively, for KU812 leukemic cells and this analysis confirmed the colocalization. On the contrary,

CC between PCL NPs and ER-Tracker was around  $0.12 \pm 0.02$  confirming low colocalization.

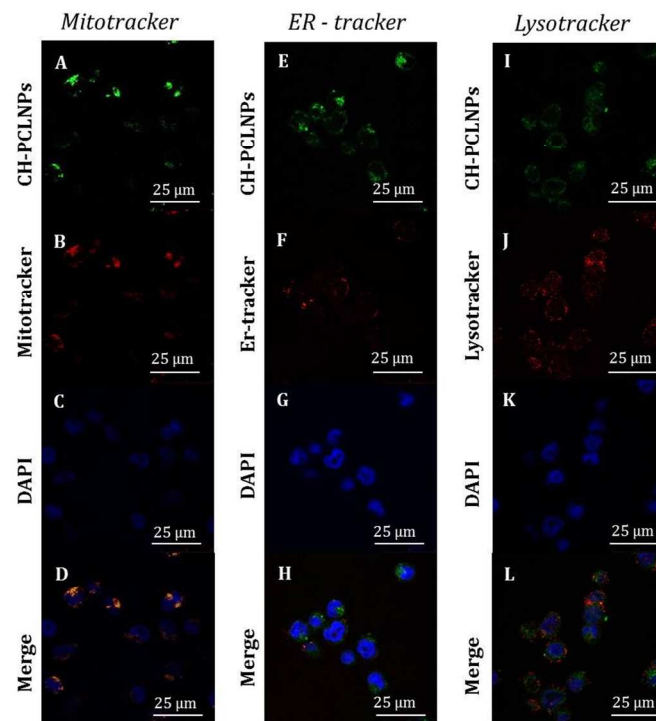


**Fig. 6.** Subcellular localization of CH-FITC loaded PCL NPs in KU812 leukemia cells (A,E,I, green). CLSM images of cell staining with MitoTracker (B, mitochondria marker, red), ER-tracker (F, endoplasmic reticulum marker, red) and Lyso-tracker (J, lysosome marker, red). In D,H,L images are shown colocalization of CH-FITC loaded NPs (A,E,I) with MitoTracker (B), ER-tracker (F) and Lyso-tracker (J) after 3 hours treatment with the nanoparticles, respectively. Cell nuclei were counterstained with DAPI (blue) as shown in the CLSM images C,G,K. 63X oil immersion objective. Scale bars: 25  $\mu\text{m}$

A common characteristic of a nanoparticles-based drug delivery systems is the rapid internalization and intracellular localization into acid endosomes/lysosomes.<sup>43,44,45,46</sup> Due to this mutual pathway of cellular uptake, there has been important interest in methods to engineer acid-triggered response from drug delivery systems for sustained intracellular release of therapeutics.

### Apoptotic response and sustained BCR-ABL inhibition

To explore the sustained killing of CML cells at nanomolar therapeutic dosage of the IM-CH loaded PCL NPs, KU812 leukemia cells and healthy C13895 cells were cultured with IM at different concentrations (10-100 nM) and IM loaded NPs with same drug dose for 1, 2, 3 and 8 days. Cytotoxicity results were valued by MTT assay (**Fig. 7**). No hostile effects on healthy C13895 cells was detected by using free or encapsulated IM at 100 nM (**Fig. 7B**). For IM loaded CH-PCL NPs, we observed a dose-dependent antiproliferative effect. Leukemic cells incubated with the equivalent doses of free IM in the medium, showed a inhibition kinetics of proliferation much slower that declined with time (**Fig. 7A**). The amounts of IM loaded in CH-PCL NPs are considerably minor than the  $\text{IC}_{50}$  value than for KU812 cells is between 100-300 nM, this clarified why apoptosis of KU812 cells was only marginally improved (20%) by using free IM at 10 nM (**Fig. 8B**) consistent with an incomplete inhibition of BCR-ABL phosphorylation/activation

that can be cancelled up to 8 days (**Fig. 8C**), while total BCR-ABL protein levels remained unaffected.

On the contrary, IM-CH loaded PCL NPs enhanced the drug's kinetics and efficiency, producing a long-lasting inactivation of BCR-ABL activity that is mandatory to significantly promote leukemia cell death and growth inhibition (**Fig. 7A-8B**). The durable inhibitory effect of IM-CH loaded PCL NPs could be due to their improved effectiveness in preventing BCR-ABL autophosphorylation compared with IM free or IM loaded PECs, without altering the total protein levels of BCR-ABL (**Fig. 8C**). The core-shell PCL NPs could provide to allow controlled release of IM and enhance its chemotherapeutic efficiency, combining the pH sensibility of CH and the slow degradation of PCL. Whereas the spontaneous intracellular degradation of PECs under physiological conditions, mediated by the presence of biodegradable dextran polyelectrolytes that was sensible to the action of intracellular proteases promote the IM release and the inhibition of BCR-ABL protein kinase activity until all polyelectrolytes were degrade.<sup>11</sup>

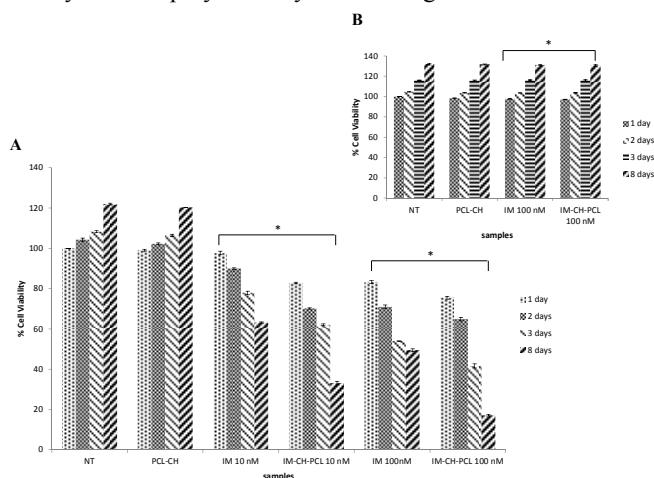


**Fig. 7.** MTT test for cellular viability of KU812 leukemia cells (A) and C13895 control cells (B) cultured for 1, 2, 3, 8 days in the absence (NT) or in the presence of CH-PCL, free IM (10 -100 nM) and IM-CH loaded in PCL NPs. Representative measurements of three distinct sets of data have been reported; \* indicates *P-values* of <0.05 for *t-Student test* between treatment groups.

Supplementary signal of apoptosis induction by IM free and IM-CH loaded PCL NPs at the dose to 10 nM in KU812 leukemia cells was confirmed by DNA fragmentation (**Fig. 8A**). DNA fragmentation is largely considered as a characteristic feature of apoptosis. **Fig. 8A** clearly indicates that the high DNA laddering pattern in KU812 leukemia cells treated with IM-CH loaded PCL NPs, liken to IM free.

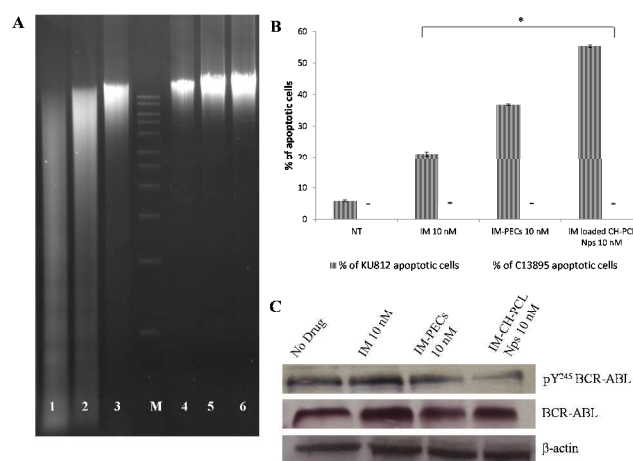


**Fig. 8.** (A) DNA fragmentation assay of KU812 leukemic cells (lanes 1-3) and C13895 healthy cells (lanes 4-6) treated for 12 hours with free IM (10 nM, lanes 1,4), IM-CH loaded in PCL NPs (10 nM, lanes 2,5). Lanes 3,6 represent the control untreated cells and lane M represent DNA marker. (B) Percentage of apoptotic KU812 leukemic and C13895 healthy cells after 72 hours of incubation with 10 nM of IM free or 10 nM of IM-CH loaded PCL NPs. Representative measurements of three distinct sets of data have been reported; \* indicate *P-values* of <0.05 for *t-Student test* between treatment groups. (C) Western Blotting analysis for the expression (anti BCR-ABL) and phosphotyrosine activation levels (anti pY<sup>245</sup> BCR-ABL) of the oncoprotein BCR-ABL in KU812 cells cultured for 8 days in the absence (No drug), in the presence of IM free (10 nM), IM loaded in PECs (10 nM) and IM-CH loaded PCL NPs (10 nM). Anti  $\beta$ -actin was used as loading control.

It is apparent that IM and IM-CH loaded PCL NPs could arrest the growth of CML cells and cause more important morphological changes, indicating an increased probability in cell death. The May-Grunwals-Giemsa staining of leukemic KU812 cells after treatment with IM free or loaded in PCL NPs (**Fig. 9B,C**) indicate a significant morphological evidence of apoptosis in the cells treated IM-CH loaded PCL NPs. In addition, fluorescent microscopy study on leukemic KU812 cells treated with IM free or loaded in PCL NPs was performed using AO/EtBr (**Fig. 9D,E,F**) and Hoechst nuclear stain (**Fig. 9G,H,I**). AO/EtBr staining cells observed as orange cells are apoptotic, while necrotic cells were observed as red colour due to their loss of membrane integrity.<sup>47</sup> The Hoechst nuclear staining cells had intact round nucleus and had normal morphology emitted a weak blue fluorescence (**Fig. 9G**), additionally the cells treated with IM-CH loaded in PCL NPs exhibited bright blue colour emission concluding nuclear fragmentation with increased chromatin condensation leading to induction of apoptosis. On the contrary, any evidence of apoptosis was observed in healthy C13895 cells (see **supplementary Fig. S9**).

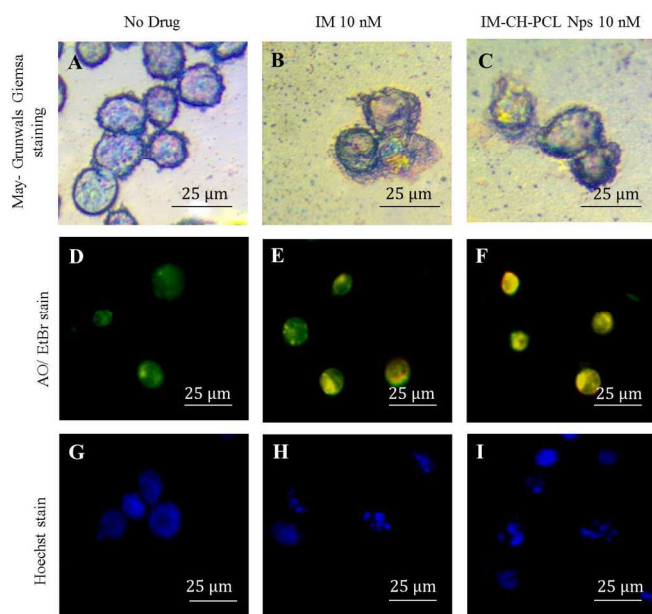


**Fig. 9.** May-Grunwals-Giemsa (A,B,C), AO/EtBr (D,E,F) and Hoechst (G,H,I) staining of KU812 leukemia cells after 72 hours of treatments, untreated cells as control (A,D,G), KU812 treated with 10 nM of IM free (B,E,H) or 10 nM of IM-CH loaded PCL NPs (C,F,I). 50X objective. Scale bars: 25  $\mu$ m.

## Conclusions

In the present study, IM-CH loaded PCL nanoparticles were formulated revealing pH-responsive drug release from the chitosan and PCL shell, considerably enhanced by decreasing pH from 7.4 to 4.0. The effective inhibition of the activity of the BCR-ABL tyrosine kinase was assessed by Western Blot analysis to 8 days of incubation with the IM-CH loaded PCL NPs with 10 nM of drug and the same concentrations of IM free. Using free IM or loaded in PECs at 10 nM we observed a partial/intermittent inhibition of BCR-ABL protein kinase activity that can be cancelled with time, as judged by an immunoprolifiling with antibodies against phospho-tyrosine BCR-ABL and its total protein levels. Conversely, by using IM-CH loaded PCL NPs to reach a final 10 nM drug concentration *in vitro*, KU812 cell viability was irreversibly blocked indicating that IM loaded in a core/shell structure improved drug's kinetics and efficacy, combining the pH sensibility of CH and the slow degradation of PCL, at single cell level consistent with a long-lasting inactivation of BCR-ABL autokinase activity that is mandatory to promote cell death. This system offers an improved alternative for the current CML therapies by reducing the dose of IM required to reach therapeutic efficacy by using single administration as opposed to multiple doses.

## Acknowledgements

This study was supported by MAAT - Nanotecnologie molecolari per la salute dell'uomo e l'ambiente (PON R&C 2007-2013, project's code PON02\_00563\_3316357). No writing assistance was utilized in the production of this manuscript. The authors have no competing interests to disclose.

## Notes and references

<sup>a</sup>Institute Nanoscience CNR (NNL, CNR-NANO) via Arnesano, Lecce, Italy;  
<sup>b</sup>Department of Physics, University Sapienza, P. le A. Moro 5, Rome, Italy;  
<sup>c</sup>Dept. Matematica e Fisica 'Ennio De Giorgi', University of Salento, via Monteroni, Lecce, Italy;  
<sup>d</sup>Italian Institute of Technology (IIT) - Center for Biomolecular Nanotechnologies, via Barsanti, Arnesano, Italy  
<sup>e</sup>Corresponding author contact - Mail: [ilariaelena.palama@nano.cnr.it](mailto:ilariaelena.palama@nano.cnr.it)

- N. Sharma, H. Dua, D. Roshia, *J. Assoc. Physicians India*, 2012, **60**, 47.
- C. Lin, Y. Li, *Cancer Cell. Int.*, 2013, **13**, 13.
- A. Bennour, I. Ouahchi, B. Achour, M. Zaier, Y.B. Youssef, A. Khelif, A. Saad, H. Sennana, *Med. Oncol.*, 2013, **30**, 348.
- D.L. Barnes, J.V. Melo, *Cell Cycle*, 2006, **5**, 2862.
- D.S. Krause, R.A. Van Etten, *N. Engl. J. Med.*, 2005, **353** (2), 172.
- P. le Coutre, E. Tassi, M. Varella-Garcia, *Blood*, 2000, **95**, 1758.
- H.G. Jørgensen, T.L. Holyoake, *Biochemical Society Transactions*, 2007, **35** (5), 1347.
- S.Y. Shieh, M. Ikeda, Y. Taya, C. Prives, *Cell*, 1997, **91**, 325.
- I.E. Palamà, S. Leporatti, E. De Luca, C. Gambacorti-Passerini, N. Di Renzo, M. Maffia, R. Rinaldi, G. Gigli, R. Cingolani, A. M.L. Coluccia, *Nanomedicine*, 2010, **5**, 4195.
- I.E. Palamà, M. Musarò, A.M.L. Coluccia, S. D'Amone, G. Gigli, *Journal of Drug Delivery*, 2011, **1**.
- I.E. Palamà, A.M.L. Coluccia, G. Gigli, *Nanomedicine*, 2013, doi: 10.2217/NNM.13.147.
- W.J. Stark, *Angew. Chem.*, 2011, **50**, 1242.
- A.D. Dinsmore, M.F. Hsu, M.G. Nikolaidis, M. Marquez, A.R. Bausch, D.A. Weitz, *Science*, 2002, **298**, 1006.
- S. Mandal, M. Sathish, G. Saravanan, K.K.R. Datta, Q. Ji, J.P. Hill, H. Abe, I. Honma, K. Ariga, *J. Am. Chem. Soc.*, 2010, **132**, 14415.
- Y. Li, X. Li, Y.S. Wong, T. Chen, H. Zhang, C. Liu, W. Zheng, *Biomaterials*, 2011, **32**, 9068.
- R. Haag, F. Kratz, *Angew. Chem.*, 2006, **45**, 1198.
- A. Nori, J. Kopecek, *Adv. Drug Delivery Rev.*, 2005, **57**, 609.
- S.W. Choi, Y. Zhang, Y. Xia, *Angew. Chem.*, 2010, **49**, 7904.
- R. Guillet-Nicolas, A. Popat, J.L. Bridot, G. Monteith, S.Z. Qiao, F. Kleitz, *Angew. Chem.*, 2013, **52** (8), 2318.
- Y. Li, W. Xiao, K. Xiao, L. Berti, J. Luo, H.P. Tseng, G. Fungand, K.S. Lam, *Angew. Chem.*, 2012, **51**, 2864.
- K. Riehemann, S.W. Schneider, T.A. Luger, B. Godin, M. Ferrari, H. Fuchs, *Angew. Chem.*, 2009, **48**, 872.
- Y. Zhu, W. Meng, H. Gao, N. Hanagata, *J. Phys. Chem. C*, 2011, **115**, 13630.
- J.L. Wu, F. Qin, F.Y.F. Chan, G. Cheng, H. Li, Z. Lu, R. Chen, *Mater. Lett.*, 2010, **64**, 287.
- Y. Wang, Y. Yan, J. Cui, L. Hosta-Rigau, J.K. Heath, E.C. Nice, F. Caruso, *Adv. Mater.*, 2010, **22**, 4293.
- M.D. Bhavsar, M.M. Amiji, *AAPS Pharm Sci Tech*, 2008, **9**, 288.
- D. Schmaljohann, *Advanced Drug Delivery Reviews*, 2006, **58**, 1655.
- P. Le Coutre, L. Mologni, L. Cleris, *J. Natl Cancer Inst.*, 1991, **91**, 163.
- E.M. Manders, J. Stap, G.J. Brakenhoff, R. van Driel, J.A. Aten, *J. Cell Sci.*, 1992, **103**, 857.
- Q. Li, A. Lau, T.J. Morris, L. Guo, C.B. Fordyce, E.F. Stanley, *J. Neurosci.*, 2004, **24**, 4070.
- E.M. Manders, F.J. Verbeek, J.A. Aten, *J. Microsc.*, 1993, **169**, 375.
- M.A. Silver, M.P. Stryker, M.P., *J. Neurosci. Meth.*, 2000, **94**, 205.
- S.V. Costes, D. Daelemans, E.H. Cho, Z. Dobbin, G. Pavlakis, S. Lockett, *Biophys. J.*, 2004, **86**, 3993.
- H. Zhang, C. Wang, B. Chen, X. Wang, *Int. J. Nanomed.*, 2012, **7**, 242.
- M. Savona, M. Talpaz, *Nature Reviews Cancer*, 2008, **8**, 341.

- 35 M. Deininger, E. Buchdunger, B.J. Druker, *Blood*, 2005, **105**, 2640.
- 36 R. Misra, S.K. Sahoo, *Eur. J. Pharm. Sci.*, 2010, **39**, 152.
- 37 E.B. Garon, L. Marcu, Q. Luong, O. Tcherniantchouk, G.M. Crooks, H.P. Koeffler, *Leuk. Res.*, 2007, **31**, 643.
- 38 I.A. Khalil, K. Kogure, H. Akita, H. Harashima, *Pharmacol. Rev.*, 2006, **58**, 32.
- 39 S. Mayor, R.E. Pagano, *Nat. Rev. Mol. Cell. Biol.*, 2007, **8**, 603.
- 40 A. Verma, F. Stellacci, *Small*, 2010, **6**, 12.
- 41 M. Ehrlich, W. Boll, A. Van Oijen, *Cell*, 2004, **118**, 591.
- 42 L. Pelkmans, A. Helenius, *Traffic*, 2002, **3**, 311.
- 43 J. Panyama, V. Labhasetwar, *Advanced Drug Delivery Reviews*, 2003, **55**, 329.
- 44 S. Ganta, H. Devalapally, A. Shahiwala, M. Amiji, *Journal of Controlled Release*, 2008, **126**, 187.
- 45 H. Kamada, Y. Tsutsumi, Y. Yoshioka, Y. Yamamoto, H. Kodaira, S. Tsunoda, T. Okamoto, Y. Mukai, H. Shibata, S. Nakagawa, T. Mayumi, *Clin. Cancer Res.*, 2004, **10**, 2545.
- 46 F. Kratz, U. Beyer, T. Roth, N. Tarasova, P. Collery, F. Lechenault, A. Cazabat, P. Schumacher, C. Unger, U. Falken, *J. Pharm. Sci.*, 1998, **87**, 338.
- 47 R. Vivek, R. Thangam, K. Muthuchelian, P. Gunasekaran, K. Kaveri, K. Kannan, *Process Biochem.*, 2012, **47**, 2410.